UC Irvine
UC Irvine Previously Published Works

Title

Building wake dispersion at an Arctic industrial site: Field tracer observations and plume model evaluations

Permalink

https://escholarship.org/uc/item/3b07d4vq

Journal

Atmospheric Environment Part A General Topics, 24(9)

ISSN

0960-1686

Authors

Guenther, Alex
Lamb, Brian
Allwine, Eugene

Publication Date

1990

DOI

10.1016/0960-1686(90)90326-i

Copyright Information

Peer reviewed

BUILDING WAKE DISPERSION AT AN ARCTIC INDUSTRIAL SITE: FIELD TRACER OBSERVATIONS AND PLUME MODEL EVALUATIONS

Alex Guenther, Brian Lamb* and Eugene Allwine

Laboratory for Atmospheric Research, Department of Civil & Environmental Engineering, Washington State University, Pullman, WA 99164-2910, U.S.A.

Abstract—Ten multi-hour atmospheric dispersion SF_6 tracer experiments were conducted during October and November of 1987 near a large oil gathering facility in the Prudhoe Bay, Alaska, oilfield reservation. The purpose of this study was to investigate dispersion under arctic conditions and in situations where building-generated airflow disturbances dominate downwind distributions of ground level pollutant concentrations. This was accomplished with a network of micrometeorological instruments, portable syringe tracer samplers, continuous tracer analyzers, and infrared visualization of near source plume behavior.

Atmospheric stability and wind speed profiles at this arctic site are influenced by the smooth (surface roughness = 0.03 cm), snow covered tundra surface which receives negligible levels of solar isolation in winter. The dispersion of pollutants emitted from sources within the oil gathering facility, however, is dominated by the influence of nearby buildings when high winds generate elevated ground level concentrations. An order of magnitude increase in maximum ground level concentration was observed as wind speeds increased from 5 to 8 m s^{-1} and another order of magnitude increase was observed as winds increased from 8 to 16 m s^{-1}. Variation in maximum concentrations was also observed with changes in wind direction. Vertical plume diffusion (σ_z) near the buildings was a factor of 2–3 greater than that observed in open terrain and was dependent on both wind speed and the projected building width and location of nearby buildings. Wind tunnel tracer distributions for east winds agree with field observations but also indicate that a significant increase in plume downwash occurs with other wind directions. Concentration distributions were calculated using several versions of the Industrial Source Complex (ISC) model. Model estimates of ground level concentrations were within a factor of three depending on wind direction. The model predictions are extremely sensitive to the ratio of plume height to vertical plume diffusion which is significantly influenced by a complex aerodynamic wake in the field.

Key word index: Arctic, dispersion, tracer, downwash, buildings, plume rise, ISC.

1. INTRODUCTION

The development and evaluation of air quality modeling techniques have greatly benefited from transport and diffusion field studies. These include early experiments using smoke visualization techniques (Richardson, 1920); the classical large scale, open terrain diffusion experiments such as Project Prairie Grass (Haugen, 1959) which provide the empirical basis for the Pasquill–Gifford (PG) curves used in current regulatory air quality models; and more recent investigations of sites and conditions which deviate from the relatively simple dispersion environment of earlier experiments. In this paper we present the results of a field tracer investigation of plume transport and diffusion near the clustered and interconnected buildings of an arctic industrial complex. The natural gas compressor turbine which was the focus of this field study is typical of the major NO_x sources in the Prudhoe Bay, Alaska, oilfields. Accurate simulation of pollutant dispersion from existing sources will aid in determining the present air quality within this tundra ecosystem and is needed for predicting the impacts of future development within potential oilfields along the Alaska coast.

We have previously analyzed open terrain micrometeorological and tracer data collected at Prudhoe Bay to provide a description of the Arctic atmospheric boundary layer (Guenther and Lamb, 1990). Near the oil gathering facilities, building-generated disturbances to the flow field around the exhaust stacks significantly change dispersion patterns by altering mean airflow streamlines and by increasing turbulence levels. Maximum concentrations can increase significantly as high winds generate downwash conditions around the low turbine and heater stacks typical of an arctic industrial complex. Field observations of plume behavior from a 35 MHP turbine are described and compared to our analysis of a wind tunnel simulation of the same source and surrounding buildings (Guenther et al., 1989). Building downwash, diffusion, and plume rise algorithms in existing Gaussian plume models and cavity wake models are evaluated in this

---

*To whom correspondence should be addressed.

paper by calculating overall model performance statistics and by considering the ability of individual model algorithms to simulate the observed dispersion process.

2. DESCRIPTION OF THE FIELD STUDY

The field tracer investigation was conducted at an oil gathering center in the Prudhoe Bay oilfield reservation. This oilfield has been in production for over 10 years and is located on the Arctic Coastal Plain of Northwestern Alaska which contains additional potential oilfields. The area is characterized by flat terrain with a very gradual slope ($\approx 0.1\%$). The continual presence of a snow covering between September and May provides a smooth surface over the short tundra vegetation. During the early winter study period (from 23 October to 9 November 1987), conditions included light winds and a strong temperature inversion as well as a winter storm with wind speeds up to $18 \, \mathrm{m \, s^{-1}}$ and blowing, drifting snow. The Beaufort Sea was frozen out to 10–20 km from the coast (Hanzlick et al., 1988) during the study, and a roughness length of 0.03 cm was measured for the snow covered tundra surface within the oilfield. A more detailed description of the field site topography, climatology, and boundary-layer meteorology is provided by Guenther and Lamb (1990).

A continuous point source was simulated by releasing a tracer gas, sulfur hexafluoride (SF_6), at a steady rate from an operating 35 MHP turbine during a series of eight multi-hour experiments (a total of 44 h). Open terrain, ground level releases were conducted during an additional two tests. The 35 MHP turbine is representative of major NO_x sources in Prudhoe Bay. Tracer concentrations were measured using syringe samplers and continuous tracer analyzers. An infrared (i.r.) video system provided near source visualization of the hot turbine stack plume. Measurements of the airflow directly upwind and within the wake of the gathering center complex were made with Gill propeller UVW anemometers. The approach flow was characterized by observations of solar insolation at 1 m, wind speed and temperature at four heights between 1 and 17 m, and wind speed and direction at thirteen heights between 60 and 450 m.

The 35 MHP turbine is located in unit 460 of Gathering Center 2 and is shown in Fig. 1 relative to the other buildings in the gathering center. The 39 m tall stack has an inside diameter of 3.6 m and is adjacent to the unit which contains the turbine. With a height of 34 m, this 20 m × 39 m wide unit is one of the highest in the gathering center complex. Figure 1 demonstrates that the building complex is highly clustered and interconnected. It is very likely that the airflow near at least some of the various pollutant sources within the complex are influenced by a number of nearby buildings.
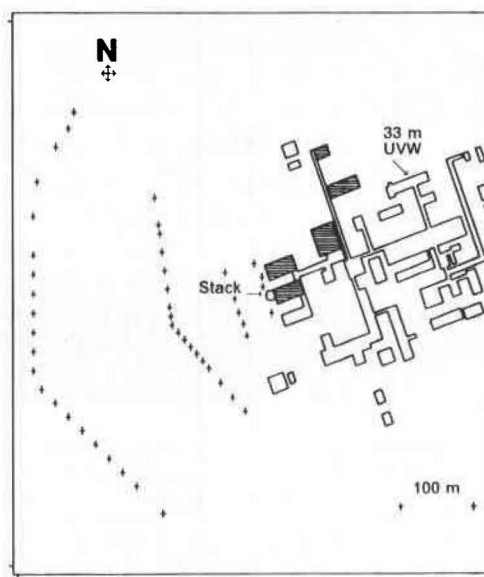

Fig. 1. Map of the GC2 oil-gathering complex showing location of the turbine stack, upwind UVW anemometer, and samplers (+) near the stack and at the 150-m and 350-m downwind arcs. Hatched buildings are 20–35 m tall whereas all others are about 20 m.

The significant buoyancy and momentum forces of the turbine exhaust were determined by monitoring hourly averaged temperature and velocity. Stack gas temperature was recorded with an iron–constant thermocouple inserted 30 cm into the stack through a sampling port at approximately half the stack height. The exhaust gas velocity was measured at the same point using a pitot tube (36″) coupled to a TDI pressure transmitter. The behavior of the plume within 15 m downwind of the stack was observed during most test periods using an infrared (i.r.) radiometer video system and recorded with a standard video recorder system. The video signals were later digitized and hourly averaged plume rise was determined using an image analysis system and standard geometrical rotation and translation equations. Monitoring of turbine exhaust thermal patterns successfully provided an inexpensive means of visualizing near stack plume behavior and is described by Rickel et al. (1990).

Hourly averaged air samples were collected with portable syringe samplers (Krasnec et al., 1984) deployed at up to 60 locations in an array of three to five sampling arcs. While the locations of the samplers ranged from 20 m to 3 km downwind, most samples were deployed on arcs between 130 and 750 m. Two of these arcs and a set of near stack sampling locations are shown in Fig. 1. Samples were analyzed with portable electron capture gas detectors located in a nearby field lab. The detection limit of this system is approximately 1 part per trillion (ppt). Ground level tracer concentrations were also measured with two fast response, continuous SF_6 analyzers (Benner and

Lamb, 1985) which were installed in vehicles and used to collect concentration records at a rate of 1 Hz for several hours at various locations during most test periods. The continuous analyzer has a response time of 0.36 s with a sample flow rate of $70\,\mathrm{cm^3\,min^{-1}}$ $(1.17\,\mathrm{cm^3\,s^{-1}})$.

The undisturbed Arctic boundary layer was probed using meteorological instruments which were located near oil well pads within 4 km of the oil gathering center and operated on a nearly continuous basis throughout the study. A Doppler acoustic sounder (AeroVironment 2000) collected wind speed and direction data at a frequency of 0.1 Hz for thirteen 30 m windows between 60 and 450 m. Aspirated thermistors (Climet 015-5) measured temperature and cup anemometers (Climet 011-3 and 011-2b) recorded wind speed at four heights between 1 and 17 m. A pyranometer (Eppley 3-48) recorded solar insolation while a 540° wind vane (Climet 012-6c) measured mean and standard deviation of wind direction at 11 m. Analog signals from these instruments were sampled and digitized at a frequency of 1 Hz and averaged with a PC portable microcomputer at 15 min intervals. Instantaneous measurements of wind velocity components were recorded at 1 Hz during tracer release periods with a Gill propeller UVW anemometer positioned on the upwind edge of the gathering center complex at a height of 33 m as shown in Fig. 1. Additional measurements at a height of 2 m were made at various locations downwind of the gathering center complex with a second UVW propeller anemometer. Data completeness of 90% was achieved during this field study and the generally high quality of the data is described in detail by Guenther *et al.* (1988). All aspects of this work are described in a report by Guenther and Lamb (1990); the meteorological, stack, and tracer data are available on computer media.

3. TYPICAL PLUME BEHAVIOR

The source of the plume was a 39 m turbine stack adjacent to a 34 m high building. Large buoyancy $(F_b \approx 350\,\mathrm{m^4\,s^{-3}})$ and momentum $(F_m \approx 600\,\mathrm{m^4\,s^{-2}})$ fluxes resulted in significant plume rise. Our analysis of dispersion near this source is simplified by the reasonably constant stack variables. The tracer release rate varied by less then 10% during any test providing a continuous, steady state source. Although changes in heat recovery operations for the 35 MHP turbine occasionally resulted in large excursions from the monthly mean values of stack temperature, T_s $=299°$C, and stack velocity, $V_s=19.1\,\mathrm{m\,s^{-1}}$ this did not occur during any tracer release periods. Typical hourly standard deviations for these variables were $\pm2°$C and $\pm2\,\mathrm{m\,s^{-1}}$. Estimates of plume rise based on Briggs (1984) buoyancy and momentum plume rise equation using the observed stack variables and ambient temperature but holding wind speed constant at

$10\,\mathrm{m\,s^{-1}}$ varied by only 1.1 m at a downwind distance of 100 m under these steady stack conditions. This is only 1.7% of the typical total plume height (64 m).

3.1. Mean plume observations

The hourly averaged wind direction was generally from the east during the eight building tests and ranged from 22° to 112°. With east winds, the main turbine stacks are on the downwind edge of the building complex as shown in Fig. 1. Wind direction fluctuations measured at 33 m height on the upwind edge of the building complex were relatively small in the range 3° to 12° during these tests. Hourly averaged wind speeds at stack height were less than $6\,\mathrm{m\,s^{-1}}$ during all of Test 4 and 2 h of Test 7. Higher speeds between 6 and $15\,\mathrm{m\,s^{-1}}$ occurred during Tests 1, 5, 6 and most of Test 7; mean wind speeds greater than $15\,\mathrm{m\,s^{-1}}$ were measured during Tests 8, 9 and 10. The along-wind turbulent intensities ranged from 6 to 9%. Stable vertical temperature gradients were observed with winds speeds less than $5\,\mathrm{m\,s^{-1}}$. The persistence of a shallow, weak surface (1–17 m) thermal inversion was observed even for high wind speeds throughout the study and is the result of near surface cooling as the relatively warm marine air passes over the tundra surface (Guenther and Lamb, 1990). Conditions at stack height were near neutral to slightly stable when wind speeds were greater than $5\,\mathrm{m\,s^{-1}}$. The low levels of solar insolation at this high latitude site (90 W m^{-2} maximum observed) were not great enough to produce diurnal patterns of atmospheric stability or local winds.

The conditions which occurred during the field study were quite representative of the prevailing wintertime meteorology along the northern coast of Alaska. As indicated by climatological records from sites along the coast, winds occur almost entirely from the east or west. High wind speeds exist more than 40% of the time.

Meteorological conditions, predicted and observed plume rise, and maximum hourly concentrations during three representative tests (6, 7 and 10) are given in Table 1. Tracer concentration isopleths from specific hours during these tests are shown in Fig. 2. Estimates of Monin–Obukhov length and gradient Richardson number, listed in Table 1, were calculated from surface temperature and velocity gradients using the procedures outlined by Berkowitz and Prahm (1982).

The isopleths shown in Fig. 2 illustrate the general plume behavior observed in all of the tests with wind speeds greater than $5\,\mathrm{m\,s^{-1}}$. At lower wind speeds, only very low concentrations were observed in the sampling grid. During tests with higher wind speeds, maximum hourly concentrations were typically measured between 300 and 600 m downwind of the stack which is in the range of 9–17 building heights (H_B). In most cases, there was little difference in the magnitude of the maximum concentration measured along each sampling arc between 300 and 600 m downwind. For
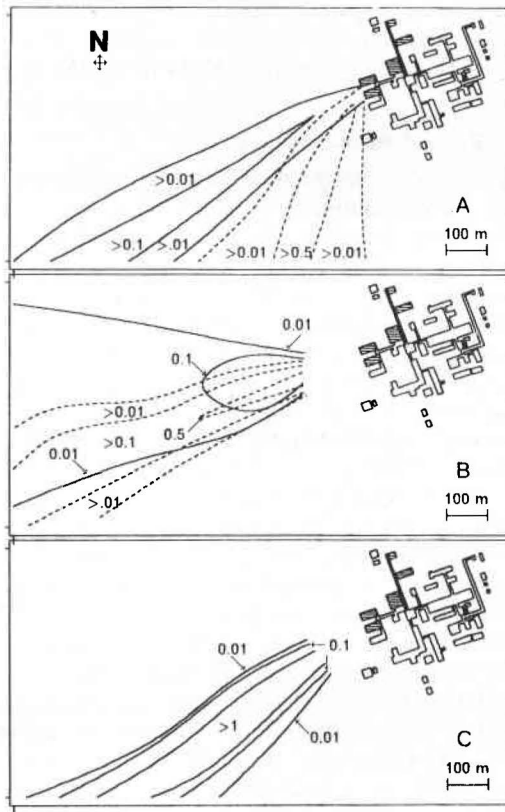
Fig. 2. Isopleths of observed ground-level, normalized hourly averaged concentration $(C/Q, \mu s\,m^{-3})$ distributions for Test 6 (A) hours 12 (solid line: $U = 8.1\,s\,m^{-1}$, $\theta = 16°$) and 14 (dashed line: $U = 8.3\,s\,m^{-1}$, $\theta = 45°$), Test 7 (B) hours 9 (solid line: $U = 5.8\,s\,m^{-1}$, $\theta = 34°$) and 14 (dashed line: $U = 11.2\,s\,m^{-1}$, $\theta = 2°$) and Test 10 (C) hour 12 (solid line: $U = 14.6\,s\,m^{-1}$, $\theta = 20°$). A wind orientation (θ) of $0°$ is normal to the smaller width of the building adjacent to the source.

example, in Test 6, hour 14, the maximum normalized concentrations (C/Q) at 150, 300 and 550 m were 0.57, 0.55 and 0.55 $\mu s\,m^{-3}$, while the maximum concentration at 750 m was 0.04 $\mu s\,m^{-3}$. This trend of relatively constant maximum concentrations with downwind distance suggests a balance between dilution of the plume due to mixing vs the effect of a descending plume centerline to bring higher concentrations toward the surface. The fact that this downwash is occurring over distances of $4–16\,H_B$ indicates that the downwash takes place beyond the boundaries of the recirculation cavity. While some of the plume is undoubtedly entrained in the recirculation cavity (high fluctuating concentrations were observed 50 m from the stack as discussed in the next section), most of the plume is apparently downwashed in the wake zone beyond the cavity. Empirical formulae derived from wind tunnel studies by Fackrell (1984a) yield a cavity length for the main turbine buildings of approximately $0.9\,H_B$ for flow perpendicular to the building (wind direction $= 70°$; approach angle $\theta = 0°$) and $1.7\,H_B$ for θ equal to $45°$. These wind tunnel studies also suggest

that the separated flow over the turbine building probably did not reattach at the roof.

During the periods listed in Table 1, several situations occurred where either the wind speed abruptly increased while the direction stayed constant or the wind direction shifted while the speed stayed constant. Since wind speed and approach angle are important parameters in plume downwash, it is useful to examine these cases further. During Test 6, hours 12–15, the wind speed was very constant at $8\,m\,s^{-1}$, but the approach angle increased from $16°$ in hour 12 to $48°$ in hour 15. The downwind distance of the maximum concentration did not show any trend with this change, but as indicated previously, there was little change in maximum concentration with distance in the touchdown area. However, the magnitude of the maximum concentration increased from 0.10 to $0.63\,\mu s\,m^{-3}$ as the approach flow angle reached $45°$. This increase indicates increased downwash with the change in approach angle. Fackrell (1984a,b), Robins and Castro (1977), and Huber (1990), among others, have demonstrated in wind tunnel studies that secondary vortices are set up from the corners of a building when the approach angle is $45°$, and that increased downwash occurs as a result of these vortices. Even though the present case represents a situation complicated by the presence of an irregular array of smaller buildings upwind of the main turbine buildings, the effect of approach angle seems to mirror the effects observed in wind tunnel studies of simple rectangular buildings.

During Test 7, hours 9–10, the wind speed was $5\,m\,s^{-1}$, but then the speed increased to a constant $11\,m\,s^{-1}$ during hours 11–15. In this case, the approach angle also changed, but it changed from $42°$ at the low wind speed to $1°$ at the high wind speed. Even though this change in angle should decrease downwash, the increase in wind speed far overwhelmed that effect and caused the maximum concentrations to increase from 0.04 to $0.50\,\mu s\,m^{-3}$. For a buoyant plume released at near building height, increased wind speed decreases the effective plume height and increases the maximum surface concentration. This effect is more obvious in comparing the maximum concentrations observed in Test 10 when wind speeds were between 14 and $16\,m\,s^{-1}$ to the maximum concentrations observed in Tests 6 and 7 when wind speeds were between 10 and $11\,m\,s^{-1}$. The concentrations increased by factors of 5–10 as the wind speed increased by 50% from approximately $10–15\,m\,s^{-1}$. The overall maximum concentration observed during the field study was $5.29\,\mu s\,m^{-3}$ and occurred during Test 10, hour 13, with a wind speed of $15.6\,m\,s^{-1}$. As shown in Fig. 3, the maximum concentration increases linearly with wind speed for the observed conditions. The reason for this relationship is shown in Fig. 3 where the relative maximum concentration (normalized by the overall test maximum concentration) is graphed vs wind speed. The observed trend is bounded very closely by a simple Gaussian plume calculation

Table 1. Meteorological conditions, observed (H_o) and predicted (H_p) plume rise, and maximum normalized concentrations

Test	Hr	U (ms^{-1})	WD (deg)	dT/dz (°C/100 m)	Ri	L (m)	σ_θ (deg)	σ_u (ms^{-1})	σ_u/U (%)	H_p (m)	H_o (m)	C_{max} (μsm^{-3})	X_{max} (m)	θ (deg)
6	09	10.5	050	1.2	0.008	486	5.1	1.8	6.5	7.0		0.72	315	20
6	10	10.6	049	1.3	0.008	502	4.6	1.7	6.9	6.9		0.99	310	21
6	11	9.5	060	1.3	0.008	201	5.5	1.8	6.3	7.6		0.27	534	10
6	12	8.1	054	1.3	0.011	355	4.9	1.9	6.7	9.1		0.10	534	16
6	13	8.4	048	1.4	0.015	260	6.7	1.8	6.4	8.8		0.20	129	22
6	14	8.3	025	1.9	0.029	123	3.6	2.2	7.2	8.8		0.63	64	45
6	15	8.3	022	2.6	0.048	68	3.2	1.8	6.4	8.8		0.41	337	48
7	09	5.3	112	2.5	0.739	<30	5.2	2.6	9.5	15.0		0.04	142	42
7	10	5.8	104	2.1	0.167	183	11.8	2.8	9.6	13.2		0.07	142	34
7	11	11.5	082	2.2	0.010	389	7.8	2.0	9.3	6.4		0.20	544	12
7	12	11.7	075	2.1	0.010	405	5.2	1.9	7.9	6.2		0.56	746	5
7	13	11.3	071	2.1	0.011	356	5.2	1.8	6.7	6.5		0.51	343	1
7	14	11.2	072	1.9	0.010	394	5.9	1.9	7.8	6.5	10.4	0.50	343	2
7	15	11.1	069	1.8	0.009	418	6.5	1.9	8.0	6.7		0.37	330	1
10	10	14.7	054	1.9	0.006	714	3.3	1.8	6.2	4.9	5.9	3.83	316	16
10	11	14.4	052	1.3	0.003	1190	3.5	1.8	6.8	5.1	5.4	3.75	316	18
10	12	14.6	050	1.2	0.003	1270	3.2	1.8	6.8	5.0	6.2	4.54	536	20
10	13	15.6	049	1.3	0.003	1290	3.1	1.8	6.3	4.6		5.29	310	21
10	14	16.0	051	1.4	—	—	3.7	1.8	6.7	4.5		4.55	536	19

H_p is from Briggs buoyancy and momentum plume rise model at 15 m from the stack; H_o at 15 m from the stack is from infrared video observations. Wind speed, direction and turbulence statistics are from hourly averaged observations at a height of 33 m on the upwind edge of GC2, while vertical temperature gradient, gradient Richardson number, and Monin–Obukhov length are from open terrain measurements at 1 m and 17 m.
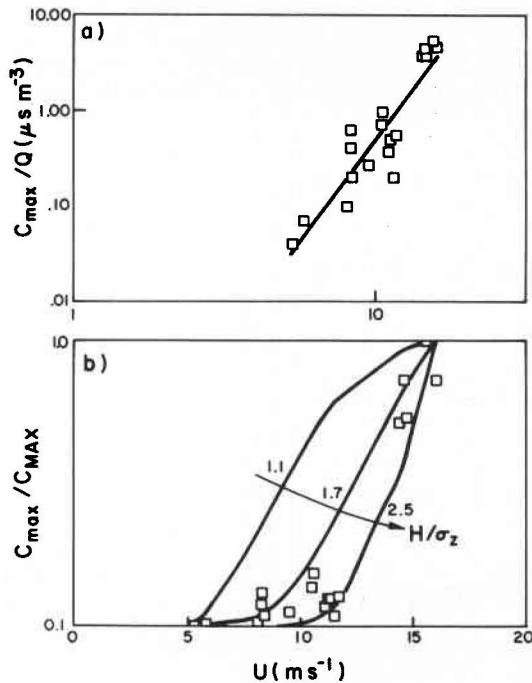
Fig. 3. (a) Normalized maximum hourly averaged concentrations (C/Q) vs hourly averaged wind speed measured at 33 m. (b) Maximum hourly averaged concentration relative to the overall test maximum ($5.29\ \mu\mathrm{s\,m}^{-3}$) vs wind speed and compared to calculated maximum concentrations for $H/\sigma_z = 1.1$, 1.7 and 2.5.

when the ratio of the plume height to the vertical diffusion coefficient (H/σ_z) is in the range 1.7–2.5. The fact that increasing this ratio from 1.1 (predicted for this situation from typical plume rise and building dispersion rate algorithms) to about 2 improves the agreement indicates the role of vertical transport—either plume rise or vertical diffusion—in determining maximum surface concentrations downwind of a building.

3.2. Plume concentration fluctuations

Measurements from the continuous tracer analyzers can be used to describe the variation in plume concentrations within each hour. Concentration fluctuation statistics for downwind locations ranging from 50 to 2300 m are given in Table 2 and include mean, peak-to-mean (top 1% of probability distribution), concentration fluctuation intensity (σ_c/C), and plume intermittence which is the per cent frequency of non-zero concentrations. Time series of instantaneous concentrations recorded near plume centerline at 540 m downwind at hour 10 of Test 6 and at 50 m downwind during hour 14 of Test 6 are shown in Fig. 4. During these 2 hs, the normalized mean was higher at 50 m ($0.81\ \mu\mathrm{s\,m}^{-3}$) than at 540 m ($0.62\ \mu\mathrm{s}$ m^{-3}), while the peak-to-mean ratio was less at 50 m (9.0) than at 540 m (13.2). During Test 6, hour 14, at 540 m downwind, the time series shown in Fig. 4a depicts several long plume events which were observed as the plume center passed over the analyzer and

resulted in a series of high concentration spikes. Between these events, smaller concentration fluctuations occurred during periods when the analyzer was near the edge of the plume and no tracer was measured when the analyzer was completely outside of the plume. For hour 10 at 50 m downwind, the concentration record in Fig. 4b demonstrated the same high concentration spikes but they are superimposed on a continuous record of low concentrations. Intermittence decreased from 94% at 50 m to 40% at 540 m while concentration fluctuation intensity increased from 96% at 50 m to 240% at 540 m. The high intermittence and low concentration fluctuation intensity at 50 m suggests a well-mixed volume which indicates the presence of a recirculation cavity out to at least this distance from the building. This was also indicated by a decrease in the turbulence intensities measured for all three wind components with a UVW anemometer at a height of 2 m from a distance of 50 m (50%) to 540 m (25%) downwind of the release stack and building.

A time series of concentrations recorded at 150 m crosswind of the mean plume centerline and 2300 m downwind of the release during hour 14 of Test 7 is shown in Fig. 4c. This continuous concentration record displays long intervals when the plume is absent interspersed with brief periods of low concentrations and small fluctuations as the internally well-mixed plume is swept over the tracer analyzer. Concentration statistics which characterize this behavior are a moderate intermittence (47%) and concentration fluctuation intensity (150%) along with a low mean ($0.13\ \mu\mathrm{s\,m}^{-3}$) and peak-to-mean ratio (6.7).

Plume intermittence at locations within 50 m of the release stack was greater than 90% and concentration intensity was less than 150% with wind speeds from 8 (Test 6) to 16 m s^{-1} (Test 9). At 540 m downwind, the location of the analyzer within the plume mean cross-section, as indicated by the results of the syringe samplers, varied from within 15 m (0.38 σ_y) of plume centerline to about 150 m (2.9 σ_y) from plume centerline. Intermittence near the mean plume edge was about 5% while concentration intensity was over 1000%. The low σ_θ observed during hour 14 of Test 6 and most hours of Tests 9 and 10 resulted in high intermittence and low concentration intensities even out to a downwind distance of 540 m from the stack.

The concentration spectra shown in Fig. 5 are typical of those observed during the study for downwind distances of 50, 540 and 2300 m downwind. A broad spectral peak occurred at a frequency of 0.05 Hz near plume centerline at downwind distances of 50 and 540 m. Huber (1988a) investigated dispersion in a wind tunnel study of a building wake and found that smoke intensity fluctuations were dominated by vortices shed by the sides and roof of the upwind building. The dominant frequencies observed at 50 m downwind during our field study, when normalized by the ratio of the velocity at a height of 0.5 H_B (17 m) in the approach flow to the height H_B (34 m), were between

Table 2. Concentration fluctuation statistics. Mean, normalized, concentration (μs m^{-3}), C, and peak-to-mean ratio, P/M^*, concentration intensity, σ_c/C, (%), intermittency, I (per cent of time that non-zero concentrations are observed) and number of seconds, N, in the record. Hourly mean wind speed, U(m s^{-1}), wind direction, WD (deg), downwind distance, DW (m) and normalized crosswind distance to mean plume centerline, CW/σ_y, are listed for reference. Time indicates the beginning of each sampling period

Test	Time	N	DW	CW/σ_y	U	WD	C	P/M	σ_c/C	I
6	9:45	599	540	0.7	10.5	50	0.26	29.7	450	24
6	10:00	3613	540	0.3	10.6	49	0.62	13.2	240	40
6	11:00	3050	540	2.9	9.5	60	0.03	22.6	1000	5
6	12:00	3933	540	1.1	8.1	54	0.10	4.5	110	76
6	14:15	3021	50	<1.0	8.3	22	0.81	9.0	96	94
7	14:30	1868	2300	1.5	11.2	72	0.13	6.7	150	47
7	15:00	2493	2300	2.5	11.1	69	0.04	13.0	250	22
8	13:00	3972	50	<1.0	17.3	68	0.56	9.1	150	97
8	14:00	3585	50	<1.0	18.4	68	0.63	7.7	130	98
10	10:15	3178	540	1.6	14.7	54	0.82	10.8	190	84
10	12:00	3646	540	0.9	14.6	50	0.72	4.4	110	98

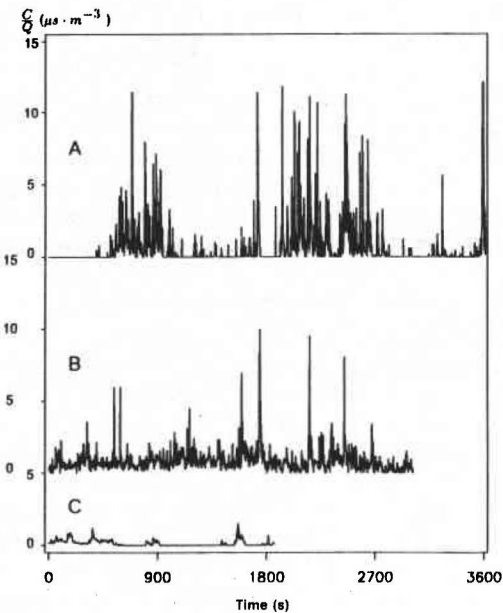* Peak concentration defined as the concentration at the 99th percentile of the frequency distribution.

Fig. 4. Time series of ground-level, normalized concentration (C/Q, μs m^{-3}) recorded at 1 Hz with fast-response, continuous SF$_6$ analyzers at 540 m downwind of the source and 15 m crosswind of the mean plume centerline during hour 10 of Test 6 (A), 50 m downwind and 10 m crosswind during hour 14 of Test 6 (B), and 2300 m downwind and 150 m crosswind during hour 14 of Test 7.

0.2 and 0.4 and are similar to the values of 0.1–0.3 observed by Huber. We observed a shift in the spectral peak to frequencies below 0.01 Hz at a downwind distance of 2300 m and crosswind distances of 150–300 m.

4. MODEL PERFORMANCE EVALUATION

4.1. Gaussian plume models

Gaussian equations are used extensively in regulatory air quality modeling applications. A point source with reflection at the ground can be modeled with the following equation:

$$C = \frac{Q}{2\pi U \sigma_y \sigma_z} \exp\left[-\frac{1}{2}\left(\frac{y-y_c}{\sigma_y}\right)^2 \right]$$

$$+ \left[\exp\left[-\frac{1}{2}\left(\frac{z-H}{\sigma_z}\right)^2 \right] \right.$$

$$\left. + \exp\left[-\frac{1}{2}\left(\frac{z+H}{\sigma_z}\right)^2 \right] \right] \tag{1}$$

where C is concentration (g m^{-3}), Q is emission rate (g s^{-1}), U is the average wind speed across the plume cross-section (m s^{-1}), σ_y is a lateral diffusion coefficient (m), σ_z is a vertical diffusion coefficient (m), y_c is the plume centerline in the horizontal plane (m), and H is plume centerline height (m). In ideal conditions, reasonable estimates of the inputs required for this equation can be obtained from measurable meteorological and source variables. Our UVW anemometer measurements near stack height provide reliable estimates of U and y_c deviated from the mean wind direction assumed in the plume models by 1°–8°. A poor estimate of y_c can result in a lack of correlation in paired observations but has little impact on bias of magnitude. Estimation of the remaining three variables (H, σ_y and σ_z), however, is difficult when they are affected by disturbances in the flow near the source. The typical plume behavior described previously demonstrate that building-generated flow disturbances have a significant impact on dispersion near the 35 MHP turbine. In this section we use our field observations to evaluate estimates of H, σ_z, and σ_y calculated with the nine algorithms (three for each variable) listed in Table 3. Uncertainties associated with the concentrations predicted by Gaussian models are considered in a statistical evaluation of the performance of the three models listed in Table 3. Each of these three models use a modified form of the Huber–Snyder equations (HSA) for calculating diffusion coefficients
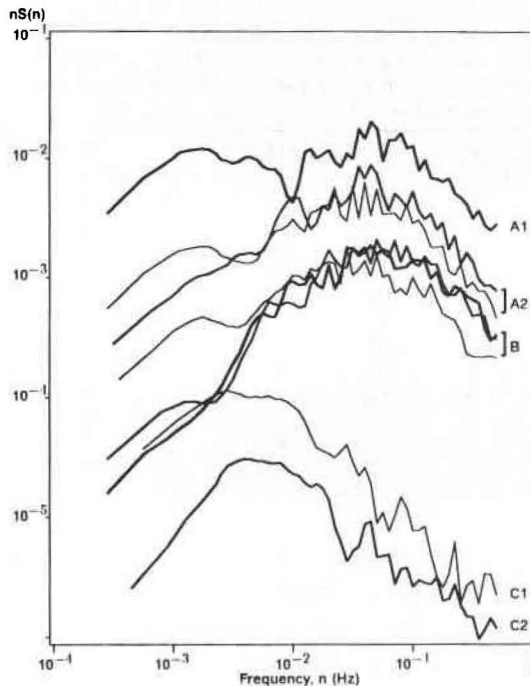
Fig. 5. Logarithmic concentration spectra for data collected at 540 m downwind and 15 m (A1) or 150 m (A2) crosswind, 50 m downwind and 10 m crosswind (B) and 2300 m downwind and 150 (C1) or 300 m (C2) crosswind.

in the building wake region and uses Pasquill–Gifford estimates outside of the wake. Each model uses one of the three different plume rise equations to estimate H.

4.2. Plume rise

The hot, high speed exhaust of the 35 MHP turbine can result in an effective plume height (H) which is significantly greater than the actual release height (H_s). This increase will greatly reduce concentrations at downwind distances where σ_z less than, but on the order of H. Table 3 indicates the three existing algorithms for estimating plume rise which we have selected from among the many methods which have been proposed. Briggs (1984) combined buoyant-momentum plume rise algorithm (BB) based on the source buoyancy flux (F_b), the source momentum flux (F_m), ambient wind speed (U), and downwind distance (x):

$$\Delta H = \frac{1.6 F_b^{1/3} x^{2/3}}{U} + \frac{1.44 F_m^{1/3} X^{1/3}}{B_m^{2/3} U^{2/3}} \qquad (2)$$

where F_b is equal to $g V_s r^2 (T_s - T_a)/T_s$, F_m is calculated as $T_a (V_s r)^2/T_s$, g is the acceleration due to gravity, V_s is stack gas velocity ($\mathrm{m\,s}^{-1}$), r is inner stack radius (m), T_s is the stack gas temperature (K), T_a is ambient temperature (K) and B_m is a momentum entrainment factor ($= 0.4 + 1.2\, u/V_s$). Scire and Schul-

Table 3. Description of the three Gaussian plume models evaluated for overall performance and the nine model algorithms which have been compared to field observations

Variable	Algorithm	Abbrev.	Equation	Reference
Plume rise (ΔH)	Briggs buoyancy	BB	(2)	Briggs (1984)
	Scire–Schulman Downwash	SS		Scire and Schulman (1980)
	Petersen–Ratcliff Integral	PI		Petersen and Ratcliff (1988)
Vertical diffusion (σ_z)	Pasquill–Gifford neutral conditions	PGD		Wagner (1987) (power law form)
	Huber–Snyder downwash	HS	(3)	Huber and Snyder (1982)
	Modified Huber–Snyder	HSA	(4)	Hanna and Heinold (1985)
Lateral diffusion (σ_y)	Pasquill–Gifford neutral conditions	PGD		Wagner (1987) (power law form)
	Lateral wind fluctuation	σ_θ	(5)	Draxler (1976)
	Huber–Snyder downwash	HS	(6)	Huber and Snyder (1982)

Model		Model algorithms		
	H		σ_z	σ_y
1	SS	Near wake:	HSA	HS
		Far wake:	PGD	PGD
2	BB	Near wake:	HSA	HS
		Far wake:	PGD	PGD
3	PI	Near wake:	HSA	HS
		Far wake:	PGD	PGD

Table 4. Model performance summary. Maximum (C_{max}) normalized concentrations ($\mu s\,m^{-3}$) and normalized mean square error (M) for wind speed ($m\,s^{-1}$), and wind orientation, θ (deg), sub-groups and for all hours combined. Because low wind speeds resulted in nearly undetectable tracer concentrations, hours with $U < 6\,m\,s^{-1}$ are not included in the θ and all hours groups. The number of samples, N, is given for each group. The M score standard deviation (σ_M) were determined using a jackknife method. The term N/A indicates that the M score could not be calculated because of mean concentrations which are close to zero

Group	Model	N	C_{max} obs.	C_{max} pred.	M	σ_m $\pm \sigma_M$
$U=2$–6	1	317	0.07	<0.01		N/A
$U=2$–6	2	317	0.07	0.15	49	190
$U=2$–6	3	317	0.07	0.040	43	15
$U=6$–13	1	512	1.96	1.43	14	2.9
$U=6$–13	2	512	1.96	10.4	52	8.3
$U=6$–13	3	512	1.96	2.43	8.6	1.5
$U=13$–18	1	662	5.29	1.74	10	1.5
$U=13$–18	2	662	5.29	15.9	7.9	1.0
$U=13$–18	3	662	5.29	8.33	3.4	0.5
$\theta=0$–10	1	466	3.17	1.55	22	4.2
$\theta=0$–10	2	466	3.17	9.24	8.7	1.3
$\theta=0$–10	3	466	3.17	8.33	7.6	1.0
$\theta=10$–30	1	633	5.29	1.74	10	1.4
$\theta=10$–30	2	633	5.29	15.9	12	1.9
$\theta=10$–30	3	633	5.29	5.58	2.6	0.4
$\theta=30$–50	1	75	0.57	0.08	50	18
$\theta=30$–40	2	75	0.57	7.44	52	18
$\theta=30$–50	3	75	0.57	0.69	8.9	6.0
All	1	1174	5.29	1.74	13.8	1.5
All	2	1174	5.29	15.9	12.8	1.5
All	2	1174	5.29	8.33	5.0	0.06

man (1980) have developed an algorithm (SS) which is similar to Equation 2 but uses a finite line source to account for a reduction in plume rise due to the initial dilution of the plume with ambient air. This method can simulate building downwash effects by making the initial plume dimensions dependent on building location and dimensions as outlined by Schulman and Hanna (1986). We used the integral plume rise equations (PI) developed by Petersen and Ratcliff (1988) as a third method of calculating plume rise. Petersen and Ratcliff have demonstrated some success in using these equations to estimate the vertical transport of buoyant plumes.

Figure 6 provides a comparison of the three plume rise algorithms and the predicted influence of wind speed and buoyancy flux. With a wind speed of $16\,m\,s^{-1}$ and a buoyancy flux of $355\,m^4\,s^{-3}$, the SS algorithm estimates a plume rise of less than 1 m at 100 m downwind, 5 m at 300 m downwind, and 21 m at 750 m downwind. The BB plume rise estimates initially grow at a much greater rate than the SS predictions and then increase at about the same rate beyond 500 m downwind. As a result, the BB plume rise estimates are about a factor of 20 greater at 100 m downwind, a factor of 7 greater at 300 m, and a factor of 3 greater at 750 m downwind. It should be noted that H is the input required for the Gaussian plume model and that these large increases in plume rise result in only 35–60% increases in H. The PI equa-

tions predict that plume rise is greater than both the SS and BB predictions at downwind distance of less than 100 m. Because the PI algorithm predicts that final plume rise is reached by 400 m downwind, the PI estimates become less than the BB estimates at downwind distances greater than 150 m and less than the SS estimates at distances beyond 850 m downwind. In the region where the highest concentrations were observed (130–750 m downwind) the PI estimates always fall in between the BB and SS estimates.

Table 1 lists several of our i.r. video field measurements of plume height at a downwind distance of 15 m. While our measurements of ΔH did not extend out to the downwind distances where Gaussian models are typically applied ($> 3H_b$) these near stack observations give a clear description of the initial downwash stage. Plume rise predicted by the Briggs equations underestimates ΔH by 5–40% in the four cases listed in Table 2 and in all other cases where plume rise measurements were made. We observed 5–6 m plume rise at 15 m downwind for $15\,m\,s^{-1}$ winds which is higher than the SS algorithm estimate at 150 m downwind. While we cannot be certain that the BB or PI estimates are accurate at 250 m downwind, it is likely that the SS predictions underestimate plume rise at least out to this distance.

The influence of buoyancy flux and wind speed was not the same for each of the three algorithms but the general trends were similar. Variation within the
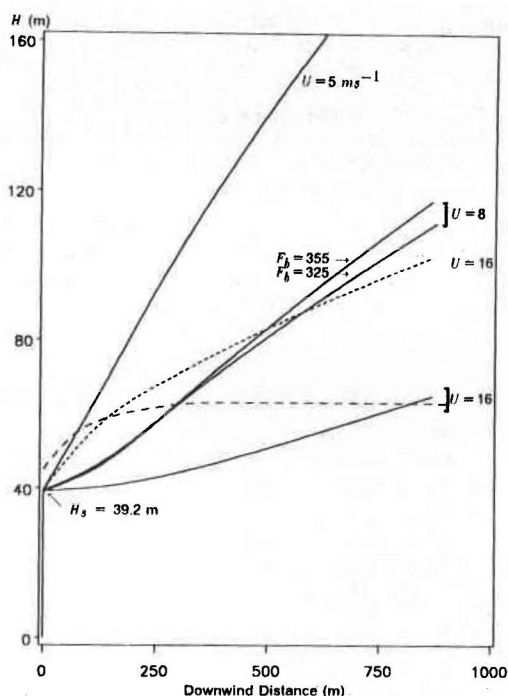
Fig. 6. Plume height (m), as a function of downwind distance (m), predicted by the BB (short dash), PI (long dash), and SS (solid), plume rise equations. The influence of buoyancy flux is demonstrated by two cases with $F_b = 325 \ \mathrm{m^4 s^{-3}}$ and $F_b = 355 \ \mathrm{m^4 s^{-3}}$, and the influence of wind speed is shown for $U = 5$, 8 and $16 \ \mathrm{m s^{-1}}$. H_s indicates the 39.2 m stack height.

limited range of buoyancy fluxes (300–$375 \ \mathrm{m^4 s^{-3}}$) observed during the field study had a small (0–15%) impact on estimates of H by the three methods tested. Figure 6 demonstrates that wind speed has a much larger impact on plume rise estimates. A decrease in wind speed from 16 to $8 \ \mathrm{m s^{-1}}$ increased the SS estimate of plume rise by about 5 m (500%) at 100 m downwind and 50 m (200%) at 750 m downwind. A further decrease to $5 \ \mathrm{m s^{-1}}$ resulted in additional increases of about 10 m at 100 m downwind and 60 m at 750 m downwind. Using our i.r. plume visualization techniques, we observed a 5 m increase in plume rise at 15 m downwind as wind speed dropped from $15 \ \mathrm{m s^{-1}}$ to $11 \ \mathrm{m s^{-1}}$.

4.3. Vertical diffusion

The Pasquill–Gifford (PG) curves are frequently used to estimate a vertical diffusion coefficient (σ_z) for Gaussian plume simulations. These curves are a function of downwind distance and discrete atmospheric stability classes and are based on empirical observations of open terrain dispersion. The high wind speed conditions observed during our study correspond to the PG curve for stability class D (neutral) which we have referred to as the PGD method in Table 3.

If the presence of a building results in turbulence levels which are significantly higher than background levels then diffusion coefficients should be increased to

simulate enhanced plume dispersion. Huber and Snyder (1982) have developed empirical algorithms, which we refer to as the HS equations, for estimating the increase in plume diffusion due to nearby buildings based on building height (H_B) and L_B which is the smaller of H_B and building width (W_B). The equation for vertical diffusion is:

$$\sigma_z = 0.5 \, L_B + 0.067(x - 3L_B). \qquad (3)$$

Huber and Snyder recommend using this equation if the source is within $2L_B$ of the building and has a plume height less than $2.5 \, H_B$ at a downwind distance of $3L_B$. In the wake region, where turbulence levels decay to background levels, the HS method increases diffusion coefficients to account for the initial increase in plume dimensions which occurred in the near-wake region. This is accomplished by adding a virtual source distance to the downwind distance used to estimate plume growth from the PG curves. Huber (1988b) used enhanced diffusion coefficients in a Gaussian model and was able to estimate ground level concentrations at the plume centerline within a factor of two for seven out of ten sets of field observations of tracer distributions near buildings. Of the 10 data sets used in Huber's evaluation, observations of dispersion from the buoyant exhaust of a natural gas compressor (Engineering Science, 1980) provided the poorest agreement and emphasizes the importance of accurately determining plume height when applying these equations to buoyant plumes with significant downwash effects.

Schulman and Hanna (1986) recommend modifying Equation 3 to linearly increase σ_z enhancement with decreasing plume height according to the following set of equations:

$$\sigma_z = A(0.7L_B + 0.067(x - 3L_B)) \qquad (4a)$$

$$\text{if } H_e \leqslant H_B \text{ then } A = 1 \qquad (4b)$$

$$\text{if } H_B < H_e < 3H_B \text{ then } A = ((H_B - H_e)/2H_B) + 1 \qquad (4c)$$

$$\text{if } 3H_B < H_e \text{ then } A = 0 \qquad (4d)$$

where H_e is the effective plume height which is equal to the sum of stack height and momentum rise determined by the equations suggested by Bowers *et al.* (1979) at $2H_B$ downwind. Schulman and Hanna also recommend using a wind direction dependent projected building width for each $10°$ interval. This method of determining σ_z within a building wake is referred to as the HSA downwash equations in this paper.

Vertical diffusion estimates from the field data are shown as a function of downwind distance in Fig. 7 along with the three algorithms (PGD, HS and HSA) listed in Table 3. These estimates were determined from field tracer distributions using a mass balance approach. This was accomplished by estimating H with the BB plume rise method and assuming a Gaussian distribution. Equation 1 can then be used to

iteratively solve for σ_z. Uncertainty in H can cause a large uncertainty in σ_z if $H \approx \sigma_z$. In these cases, using a SS plume rise method would result in 25% to 50% lower field estimates of σ_z. The HS and HSA equations estimate that σ_z increases proportional to L_B and the 14 m increase in L_B between $\theta = 0°$ wind orientation and $\theta = 20°$ winds results in the 7 m increase in σ_z illustrated by Fig. 7. L_B is constant for $\theta > 20°$ because building height is then less than the projected building width. The plume height dependent factor A in Equation 4 causes the HSA algorithm to estimate a σ_z that is several meters lower than the HS estimate when plume rise is very small due to high winds. Figure 7 shows that the HSA equation estimates of σ_z are about 10 m lower than the HS estimates when wind speed drops to 8 m s^{-1}.

The scatter in the field estimates of σ_z shown in Fig. 7 are a result of the influence of the many nearby buildings in the GC2 complex and the uncertainty in our estimate of H. This makes it difficult to quantify the influence of wind speed and direction but the

estimates clearly demonstrate that the PG neutral curve greatly underestimates σ_z. Building-enhanced diffusion near the source increases σ_z by a factor of two to three over both the PGD algorithm and observed open Arctic terrain estimates reported by Guenther and Lamb (1990). Our field estimates of σ_z tend to increase with the projected building width of the building adjacent to the source which lends support to the HS and HSA equations. Observed estimates of σ_z also tend to decrease with lower wind speed which is in agreement with the HSA algorithm.

As demonstrated previously in Fig. 3, the exponential relationship between the ratio, H/σ_z, and the concentration calculated with the Gaussian plume equation causes concentrations to be very sensitive to plume height if $H/\sigma_z > 1$. Depending on the value of this ratio, maximum concentrations predicted for a given σ_z were one to two orders of magnitude higher using H estimated with BB plume rise equation (Model 1) compared to those calculated with the SS estimate of H (Model 2).

The ground level crosswind integrated concentrations shown in Fig. 8 are a measurement of vertical dispersion (both H and σ_z). It should be noted that our
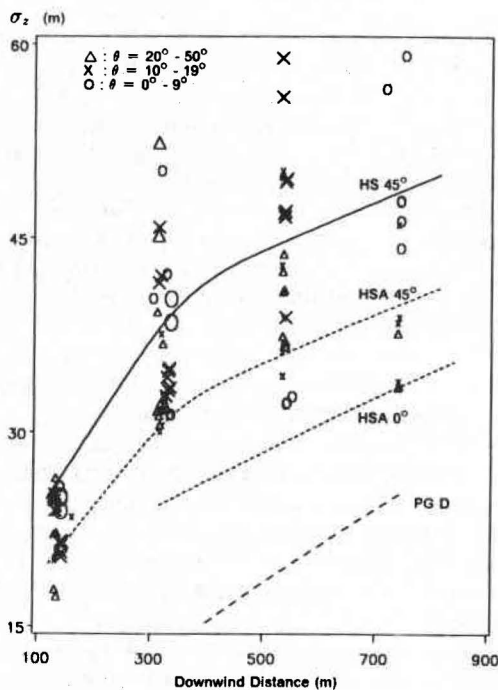

Fig. 7. Vertical plume diffusion, σ_z (m), as a function of downwind distance (m). Field estimates for each downwind arc are grouped by wind orientation and wind speed with the small symbols denoting 6–13 m s^{-1} winds and the large symbols representing 13–19 m s^{-1}. A wind orientation of $0°$ is normal to the smaller width of the building adjacent to the source. These estimates of σ_z were calculated with a mass balance approach which assumed a Gaussian distribution and the plume height predicted by Briggs combined momentum and buoyancy equation. Estimates predicted by the modified Huber–Snyder with $\theta = 0°$ and $45°$ orientations (short dash), the original Huber–Snyder with $\theta = 45°$ (solid), and the Pasquill–Gifford neutral stability (long dash) diffusion equations are shown for reference.
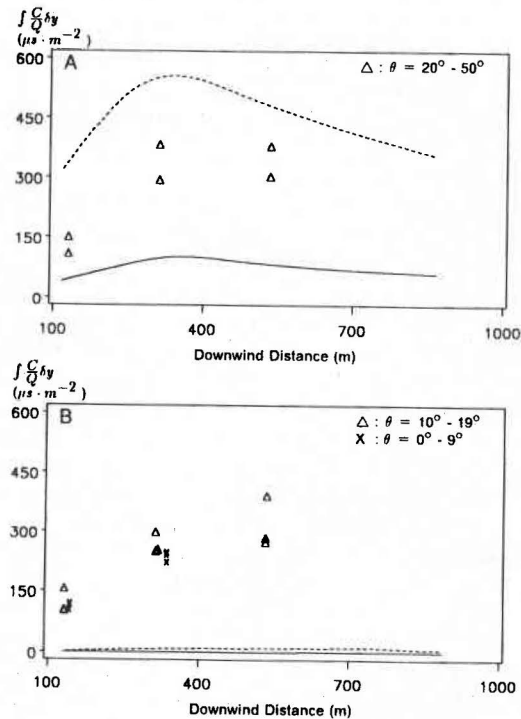

Fig. 8. Normalized hourly averaged crosswind integrated concentration, $\int C \partial y (\mu s \, m^{-2})$, as a function of downwind distance (m). Field observations for each downwind arc are shown for periods when wind speeds were greater than 13 m s^{-1}. Wind orientation categories include 20–$50°$ (A) and 0–$9°$ and 10–$19°$ (B). A wind orientation of $0°$ is normal to the smaller width of the building adjacent to the source. Estimates predicted by plume models 1 (dash) and 2 (solid) are shown for each of the three wind orientation categories at a wind speed of 16 m s^{-1}.

field estimates of the integral have a much smaller uncertainty than our estimates of σ_z because the integrated concentrations are obtained directly from the tracer data and no estimate of plume height is required. Figure 8 demonstrates that field estimates of integrated concentrations for $\theta = 20$–$50°$ fall between the values predicted by Models 1 and 2. Both the models and the field data indicate that maximum integrated concentrations tend to be between 300 and 600 m downwind. The small projected building width (20 m) which results with a $0°$ building orientation results in underpredicted estimates by both models for these cases. While there is as much as a factor of 2–3 decrease in observed integrated concentration this is much less than the predicted decrease of several orders of magnitude. The presence of many buildings surrounding the source is probably responsible for the persistent enhanced dispersion which occurs even when the building adjacent to the source has a small projected building width. The orders of magnitude decrease in integrated concentration predicted by the models is the result of a relatively small (50%) increase in σ_z which emphasizes the need for very accurate estimates of σ_z. Figure 9 illustrates that the model predictions of an increase in ground level integrated

Fig. 9. Normalized hourly averaged crosswind integrated concentration, $\int C \partial y (\mu s\,m^{-2})$, as a function of downwind distance (m). Field observations for each downwind arc are shown for low and high wind speeds when wind orientation was between 20 and $50°$. A wind orientation of $0°$ is normal to the smaller width of the building adjacent to the source. Estimates predicted by plume model 2 are shown for a $45°$ wind orientation with wind speeds of 8 and 16 m s^{-1}.

concentrations with wind speed is in agreement with the field data.

4.4. Lateral diffusion

Most Gaussian plume models determine lateral diffusion in open terrain from the PG curve for σ_y. We have selected the curve for neutral stability and refer to this method of selecting σ_y as the PGD method in Table 3. Estimates of σ_y can alternatively be based directly on wind direction fluctuations with the following equation:

$$\sigma_y = x \tan(\sigma_\theta)/(1 + X/B)^{1/2} \qquad (5)$$

where B is a spatial scale which can be estimated as the product of mean wind speed and twice the Lagrangian time scale of diffusion (Draxler, 1976). This method of estimating σ_y is referred to as the σ_θ algorithm in our analysis.

The HS diffusion algorithm listed in Table 3 provides the following equation to describe building-enhanced lateral diffusion:

$$\sigma_y = 0.35\, W_B + 0.067(x - 3H_B). \qquad (6)$$

Huber and Snyder (1982) recommended using this equation only when the effective plume height at $2H_B$ downwind is less than $1.2\,H_B$. Since this is not the case for the source we investigated, unless wind speeds are greater than 25 m s^{-1}, this equation is not applied by the HS algorithm in our analysis.

Estimates of lateral diffusion, σ_y, shown in Fig. 10 were estimated using a non-linear best fit to observed crosswind tracer distributions. The estimates fall between the PG D (neutral) and A (very unstable) curves at downwind distances of less then 500 m. Our analysis of tracer data collected in open terrain suggests that low frequency contributions to hourly lateral wind direction fluctuations can greatly increase σ_y in the field (Guenther and Lamb, 1990). Figure 11 demonstrates the impact of the σ_θ algorithm on Gaussian model estimates of maximum centerline concentration. A 30% increase (or decrease) in maximum concentration, relative to that predicted using the PGD estimates of σ_y, results when σ_θ is decreased (or increased) by $1°$.

The scatter plot of observed σ_y vs predicted σ_y shown in Fig. 12 indicates that Equation 5, with σ_θ measured at a height of 11 m and B equal to 500 m (estimated from measured Eulerian time scales), provides a slightly better estimate of σ_y than the PGD algorithm does at the short downwind distances ($\sigma_y < 40$) which are associated with maximum concentrations at this site. The enhancement of σ_y primarily in this region could be due to building generated disturbances to the flow or because of the decrease in the rate of lateral plume growth expected with longer travel times. Figure 10 shows that the HS algorithm provides a reasonable prediction of σ_y within the building wake. The addition of a factor A, similar to that used in the HSA algorithm (Equation 4), to
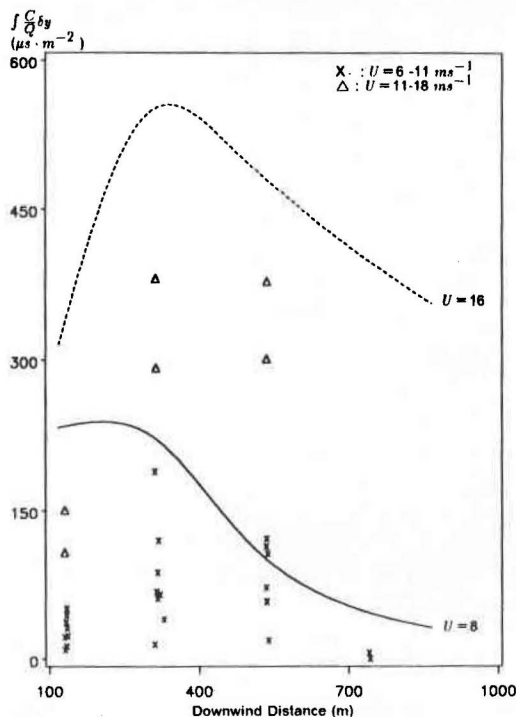
σ_y (m)

△ : θ = 20-50°
X : θ = 10 - 19°
O : θ = 0 - 9°
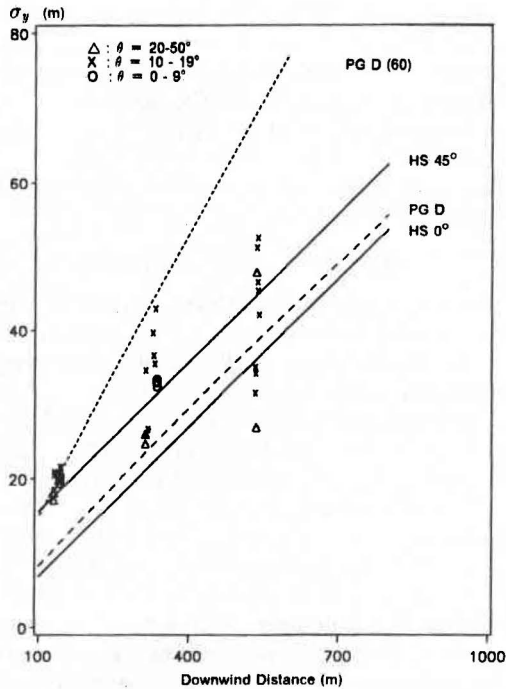
PG D (60)

HS 45°

PG D

HS 0°

Downwind Distance (m)

Fig. 10. Lateral plume diffusion, σ_y(m), as a function of downwind distance (m). Field observations for each downwind arc are shown for three wind orientation categories for periods when wind speeds were greater than 11 m s^{-1} and σ_θ was less than 5°. A wind orientation (θ) of 0° is normal to the smaller width of the building adjacent to the source. Estimates predicted by the Huber–Snyder (HS) equations with $\theta = 0°$ and 45° orientations (solid line), the Pasquill–Gifford (PG) neutral stability equation unmodified (long dash) and modified (by multiplying by a factor of 1.8) to account for a 1-h averaging time (short dash).
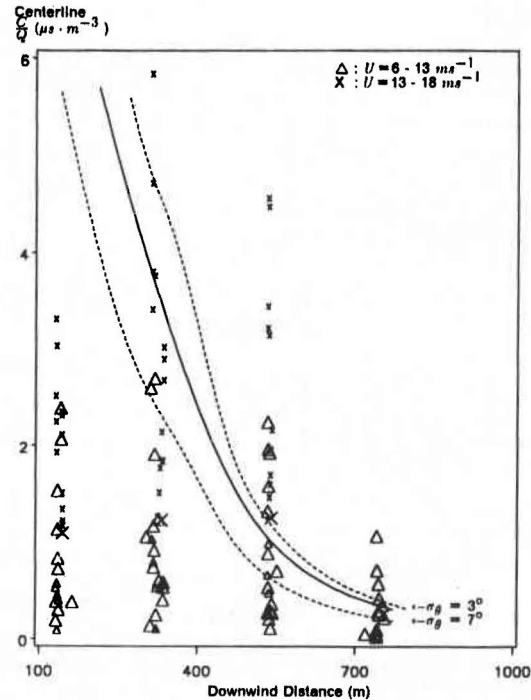

Centerline
$\frac{C}{Q}$ ($\mu s \cdot m^{-3}$)

△ : $U = 6$ - 13 ms^{-1}
X : $U = 13$ - 18 ms^{-1}

$\sigma_\theta = 3°$
$\sigma_\theta = 7°$

Downwind Distance (m)

Fig. 11. Normalized hourly averaged plume centerline concentration, C/Q ($\mu s\, m^{-3}$), as a function of downwind distance (m). Field estimates for each downwind arc are grouped by σ_θ and wind speed for cases where wind orientation (θ) was between 10 and 50°. A wind orientation of 0° is normal to the smaller width of the building adjacent to the source. Small symbols indicate $\sigma_\theta < 5°$, and the large symbols represent $\sigma_\theta > 5°$. These estimates of centerline concentration were calculated by using a nonlinear best-fit to crosswind concentration distribution profiles. Estimates predicted with model 2 for 16 m s^{-1} winds and $\sigma = 45°$ are shown with a solid line. Model-predicted influence of lateral dispersion is demonstrated by concentrations (dashed line) estimated by using σ_θ to estimate σ_y in a Gaussian plume model.

Equation 6 would provide a simple means of extending lateral building-enhanced diffusion to the plume heights we observed in the field.

4.5. Overall model performance

Our analysis of the three Gaussian model inputs (H, σ_z, and σ_y) demonstrates the difficulty in estimating these variables for the buoyant source located within the complex wake of the clustered buildings at the oil gathering center. We have quantified the performance of standard Gaussian modeling techniques with a statistical evaluation of the concentration distributions estimated by the three Gaussian plume models listed in Table 3. Each model is a version of the ISC model which is used extensively for estimating pollutant concentrations near industrial facilities similar to our test site. All three of these models use the HSA equations for estimating diffusion within the building wake region and the PGD estimates outside of the wake. The first model uses the Briggs analytical plume rise equation, model 2 uses the Schulman–Scire downwashed plume rise method and model 3 uses the Petersen integral plume rise algorithm.

The performance of the three models for each of the 44 stack test hours was evaluated by a comparison of the observed and predicted mean and maximum concentrations and the normalized mean square errors. Figure 13 illustrates the comparison of hourly maximum centerline concentrations estimated by the models and observed in the field. Model 1 tends to underestimate the maximum concentration while Model 2 tends to overestimate and Model 3 predictions fall in between. Maximum centerline concentrations estimated by Model 1 were within 10% of observed concentrations in only two cases and underpredicted by more than 10% in 42 out of the 44 cases. The lower plume rise estimated with the SS equations overpredicted maximum concentrations by more than 10% for two-thirds of the cases. Each of the remaining fourteen hours were underpredicted by more than 10% and occurred either when wind speeds were less than 6 m s^{-1} or when wind orientation was less than 10°. The small projected building width for $\theta < 10°$

Observed
σ_y (m)
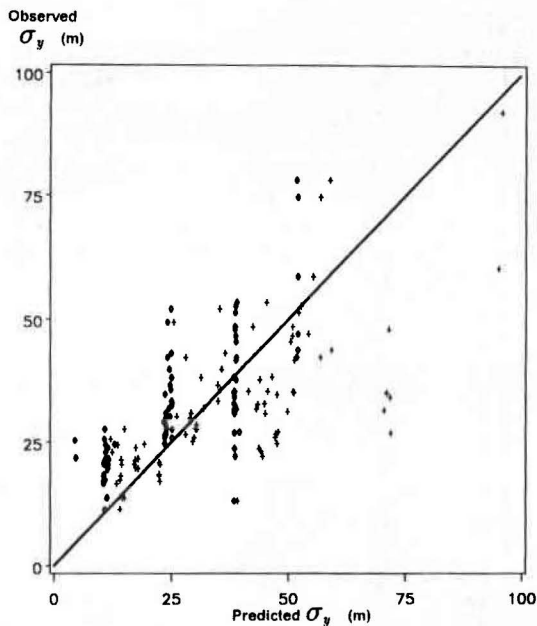

Fig. 12. Observed lateral plume diffusion (σ_y) vs estimates predicted by PG stability class D (neutral) curve ($\diamond$) and by Equation 6 (+), where σ_θ is measured at a height of 11 m and $B = 500$ m.
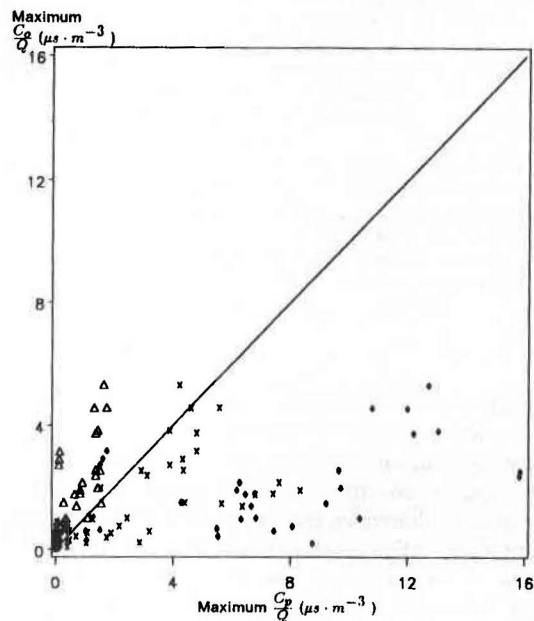
Maximum
$\frac{C_p}{Q}$ ($\mu s \cdot m^{-3}$)

Fig. 13. Ground-level, maximum observed normalized hourly averaged plume centerline concentration (C/Q_o, $\mu s\,m^{-3}$) vs maximum predicted concentration (C/Q_p, $\mu s\,m^{-3}$) with Models 1, 2 and 3 for all test hours.

building orientation results in a greatly underestimated σ_z which more than offset the underestimated plume height predicted by Model 1. This emphasizes the caution which must be used when evaluating these models since inaccurate estimates of both σ_z and H can result in the correct ratio of H/σ_z and the correct

maximum concentration. The maximum concentration predicted by Model 3 was within 10% of the observed maximum in 3 of the 44 cases, but the model underpredicted by more than 10% in 13 cases (29%) and overpredicted by more than 10% in 28 cases (64%).

The normalized mean square error (M) provides an overall score of model performance:

$$M = \overline{(C_o - C_p)^2} \cdot (\bar{C}_o - \bar{C}_p)^{-1} \qquad (7)$$

where C_o is the observed field concentration, $\bar{C}_o$ is the mean observed concentration, C_p is the concentration predicted by the plume model, and $\bar{C}_p$ is the mean predicted concentration. When the product of $\bar{C}_p$ and $\bar{C}_o$ is near zero, which occurred for some hours of test 4 and 7, the M score cannot be calculated. The M score is a function of the three statistical scores (t, F and r) which have been proposed for model performance evaluation by the EPA (1981). The t statistic is a measure of the bias of magnitude, the F statistic is a measure of the bias of variance, and the correlation coefficient (r) is a measure of the intensity of association. While a perfect model would have an M score of 0, Hanna and Heinold (1985) suggest that a very good model would have an M score less than 0.4 and a bad model would have an M score greater than 5. By this definition, poor model performance was found in most cases with Models 1 (89%), 2 (70%) and 3 (64%). The F, t and r statistics indicate that this was primarily due to a bias in magnitude rather than variability or correlation. Since no M score was less than 0.4, the very good model definition was not achieved in any of the comparisons. An intercomparison of the three models indicates that model 1 resulted in significantly better M scores, based on 95% confidence limits determined using the jackknife method outlined by Efron (1982), in three of the 44 cases. Model 2 scored significantly better than the other two models in seven cases (16%) while Model 3 scored significantly better in 17 cases (39%).

The model performance statistics listed in Table 4 show that model 3 performed significantly better than the other two models for all wind speed and wind direction categories except with a wind orientation of less than 10°. Model 2 performed much better with higher wind speeds and with a building orientation close to 0°. Models 1 and 3 displayed less variation in performance with wind speed and direction but performed somewhat better with higher wind speeds and with wind orientation between 10 and 30°. For all hours combined, Models 1 and 2 had an M score of about 13 while Model 3 had an M score of 5. These M scores are similar to those calculated by Hanna and Heinold (1985) while comparing Gaussian model predictions to the field dispersion data collected by Engineering Science (1980) near natural gas compressor stations.

We found little change in model performance when other lateral dispersion algorithms from Table 3 were

substituted for the ones used in the analysis described above. Use of the σ_θ algorithm resulted in better model performance when used with the SS plume rise equations in cases where measured σ_θ was larger than 6° (resulting in a lower maximum concentration estimated with the σ_θ algorithm) and worse model performance when σ_θ was less than 3° (resulting in higher maximum concentrations). With the BB plume rise equation, and its underestimated concentrations, the use of the σ_θ algorithm has the opposite effect—improving model performance by increasing concentrations when σ_θ is small. Vertical dispersion dominates the distribution of ground level concentrations at this site and the choice of σ_y just serves to slightly increase or decrease concentrations which are greatly under or overestimated by the various plume rise and vertical diffusion algorithms.

With the plume rise estimated by the BB plume rise algorithm, model performance can be improved significantly by using the HS diffusion equations—but this may only be due to the model sensitivity to H/σ_z creating the need for an overestimated σ_z to offset an overestimated plume height. Although our near source plume visualization in the field indicates that the BB and PI equations are more accurate for the east winds we investigated, wind tunnel results suggest that this is not the case for other wind directions. Any model we choose based strictly on statistical comparison to our field observations is not likely to give us the best performance when simulating the same source with a different wind direction. This prevents us from concluding that any combination of the model algorithms in Table 3 provides the best model performance for all conditions at this site.

A final consideration is determining how well the Gaussian equation describes the overall process of dispersion. Our analysis of wind direction fluctuations at this site, described by Guenther and Lamb (1989), indicates that while crosswind plume profiles should fit a Gaussian distribution for time periods of up to 5 min, they do not for periods of 1 h. This is due to meandering and is present to some degree at any field site. The influence of the leeward recirculation cavity, which complicates the application of Gaussian models, is described in the next section. The inherent limitations in the performance of Gaussian models, with algorithms such as those listed in Table 3, is evident in the observed variation in field concentrations shown in Fig. 12. A factor of 3 variation in concentration was observed at 320 m downwind and a factor of 4 at 540 m downwind during hours when mean wind speed was between 10.5 and 12.6 m s^{-1}, wind direction was between 42 and 48°, σ_θ was between 4.6 and 5.1°, and stack temperature varied by 6°C and stack velocity by 1 m s^{-1}. Even if the Gaussian models performed well on the average, they could not predict the variation in concentration which is observed in the field with small changes in the variables which determine model inputs.

4.6. Recirculation cavity models

In addition to predicting concentrations in the building wake region, we are also interested in concentrations which occur in the recirculation cavity immediately next to a building complex. The lack of a mean transport direction and a very non-Gaussian distribution within the recirculation cavity severely limit the ability of Gaussian plume models to predict concentration distributions within this region. Hosker (1984) assumes that the cavity is fairly well mixed so that the concentration at any point can be estimated by the following equation:

$$C = Q/(1.5\,H_B\,W_B\,U) \qquad (8)$$

where U is one-half the wind speed at stack height and the factor of 1.5 accounts for partial plume entrainment. The plume is considered partially entrained into the cavity if H_e, plume height based on momentum rise at $2H_B$, is less than cavity height estimated as:

$$H_c = H_B[1.0 + 1.6\exp(-1.3\,L/H_B)] \qquad (9)$$

where L is the alongwind dimension of the building. Values of H_c for the cavity near our release stack are less than H_e when wind speeds at stack height are greater than 8 m s^{-1}. We observed hourly averaged concentrations of 0.3–0.7 μs m^{-3} within 50 m of the stack for periods with a mean wind speed at stack height that varied from 8 to 17 m s^{-1}. Normalized concentrations of 60–240 μs m^{-3} are estimated using Equation 8, which assumes that two-thirds of the plume is entrained, and are about two orders of magnitude greater than observed mean concentrations. Time series of instantaneous concentrations indicate that the cavity was fairly well-mixed (intermittence > 80%, concentration fluctuation intensity < 150%) with maximum concentrations up to 10 μs m^{-3}.

The poor agreement we found between Gaussian plume and cavity model predictions and field observations demonstrate the need to better understand the processes controlling dispersion near pollutant sources at this arctic industrial facility. While these and similar models can be empirically modified to provide better agreement with our field data, the wind tunnel data described in the next section demonstrate that concentration distributions vary dramatically with wind direction. The observed variation is complex and it is not likely that any analytical model is capable of performing well for all of the conditions which occur at this field site.

5. COMPARISON TO WIND TUNNEL OBSERVATIONS

The Radian Corporation and NHC Wind Engineering, Inc. (1985) conducted a wind tunnel simulation of the oil gathering center we studied in the field as part of an air quality impact assessment. Our analysis

of the results of this wind tunnel study are described in detail by Guenther *et al.* (1989) and provide additional insights into dispersion at this site. We have included a discussion of the results of the wind tunnel study in this section in order to compare field and wind tunnel observations and to assess the utility of these two methods. The plume centerline concentrations observed in the wind tunnel under comparable field meteorological conditions are shown in Fig. 14 as a function of downwind distance. The general pattern of plume touchdown, indicated by centerline concentrations, at 300–500 m downwind was observed in both the field and wind tunnel experiments as well as an increase in concentration with wind direction (from northeast to east winds) and with increasing wind speed. The field concentrations are, however, 5–300% lower than the wind tunnel observations. The stack velocity used in the wind tunnel (20.1 m s^{-1}) was similar to that observed in the field but the temperature of the exhaust measured in the field was greater than that simulated in the wind tunnel (177°C) resulting in a 20% greater buoyancy flux. This accounts for a portion of the observed decrease in concentration observed in the field. Wilson and Chui (1987) suggest that an additional factor of 1.8 decrease in centerline

concentration in the field is expected due to plume meandering (deviations in horizontal wind direction at time scales between 10 min and 1 h) which occurs in the field but is not simulated in the wind tunnel. Figure 14 demonstrates that the wind tunnel and field data agree reasonably well when these two factors are taken into account.

The wind tunnel results shown in Figure 14 indicate that a change in wind direction can drastically effect pollutant distributions. The HSA equations provide the means to vary downwash effects with projected building width as a function of wind direction. Figure 14, however, suggests that building width is not the only factor controlling downwash since west and east winds have the same building orientation but very different concentration distributions. Field i.r. visualization of near stack plume behavior indicates that easterly flow did not result in a decreased plume rise due to building influences. A decreased plume rise for the north and west wind cases in the wind tunnel could have caused the higher observed concentrations which are close to those predicted with the SS downwashed plume equations.

6. SUMMARY

Building-generated airflow disturbances must be considered when estimating the ground level distribution of pollutants near Arctic industrial sites during high wind speed conditions. The source we investigated, a natural gas compressor turbine, is typical of the major sources of NO_x emissions in the Prudhoe Bay region. A very small surface roughness (0.03 cm) and a lack of solar insolation influence the approach wind speed profile and atmospheric stability at this arctic site. The resulting arctic atmospheric boundary layer can be simulated in Gaussian plume models by using site specific wind speed profiles and by selecting a stability category based on σ_θ, L or Ri rather than time of day, solar insolation, and wind speed. With the downwash conditions that result in the highest ground level concentrations at this site, dispersion is dominated by the wakes of clustered buildings near the source. This is not a situation which is not unique to the Arctic but occurs at lower latitude sites as well. The following conclusions concerning vertical and lateral dispersion and Gaussian plume model performance are relevant for similarly clustered sites.

6.1. *Plume rise and vertical diffusion*

(1) Infrared video observations of plume rise within 15 m of the stack indicate that plume rise is greatly underestimated by the Schulman and Scire downwashed plume rise equation at this distance. Downwashed predictions of plume rise at 150 m downwind are less than observed at 15 m downwind. This underestimation presumably occurs because the algorithm accounts for more plume downwash via the line source con-
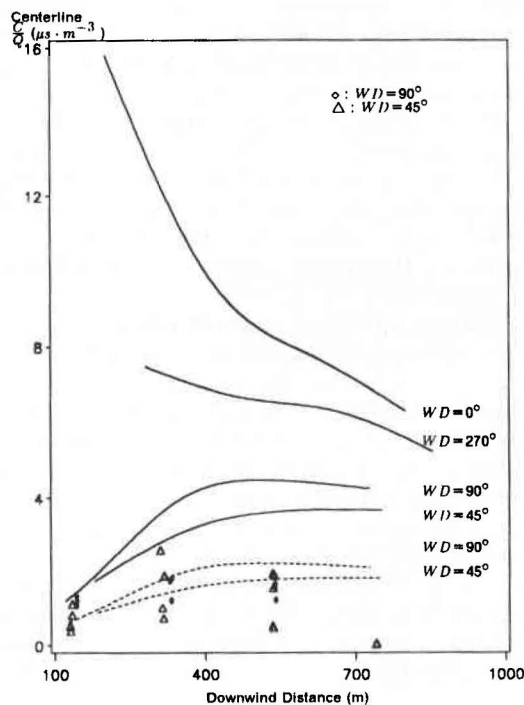

Fig. 14. Normalized centerline concentration, C/Q, (μs m^{-3}), as a function of downwind distance, observed in the wind tunnel (solid line) for north (0°), northeast (45°), east (90°) and west (270°) winds at 12 m s^{-1}. Field observations are for cases where wind speed was within 2 m s^{-1} of 12 m s^{-1} and wind direction was within 10° of either 45° or 90°. Dashed lines illustrate wind tunnel estimates for 45 and 90° winds adjusted to account for the lower buoyancy flux and increased meander observed in the field.

cept than actually occurs for the high buoyancy, high momentum turbine plume. The Briggs buoyancy equation and Petersen integral algorithm provide reasonable estimates of the observed plume rise at 15 m downwind.

(2) Estimates of σ_z have a large uncertainty ($\pm 10\%$ to $\pm 50\%$) due to uncertainty in H but the variation in σ_z with wind speed and direction is large enough to demonstrate that buildings near the source generate a significant increase in vertical dispersion. Both the original and modified Huber–Snyder equations underestimate observed vertical dispersion by more than a factor of two. Part of this underestimation is probably due to differences between the hourly averaging time in the field vs the 10 min averaging period associated with the HS wind tunnel data. The effects of a very buoyant plume to enhance dispersion could also be a factor.

(3) The modified Huber–Snyder equations predicts the observed increase in vertical dispersion with increasing wind speed, but underestimates the rate of this increase.

(4) Field observations demonstrate that vertical dispersion varies with wind direction which indicates that dispersion is influenced by projected building width and geometry. The projected width of the single building adjacent to the source, however, does not account for the observed variation. The contribution of all nearby buildings to dispersion enhancement must be considered.

6.2. Horizontal diffusion

(1) Hourly horizontal dispersion rates in open terrain tend to be larger than predicted by PG dispersion primarily due to the increased meander associated with an hourly averaging period.

(2) Horizontal dispersion rates within 10 H_B of the source were slightly larger than dispersion estimates based upon lateral wind direction fluctuations or PG estimates. Although the plume is above the region ($H \leqslant 1.2\,H_B$) recommended for the Huber–Snyder curves, these observations suggest that dispersion enhancement, perhaps due to buoyancy-induced entrainment, occurs in this situation. The enhancement of σ_y could be extended to heights above 1.2 H_B in a manner similar to the accepted method for σ_z (Equation 4).

6.3. Model performance

(1) In almost every case, the model using Briggs plume rise equation underestimated observed concentrations. Maximum concentrations were underpredicted by a factor of 2–6 in most cases. Concentrations could be increased by using the original Huber–Snyder equations. An M score of 13.8 was calculated using all test hours with $U > 6\,\mathrm{m\,s}^{-1}$.

(2) In every case, except for winds approaching normal to the smaller building width and wind speeds less than $6\,\mathrm{m\,s}^{-1}$, the model using the Schulman–Scire downwashed plume rise method overestimated observed concentrations. Maximum concentrations were overpredicted by a factor of 2–8 in most cases. Winds normal to the smaller building width, which results in a small σ_z predicted by the model, underestimated concentrations by a factor of 2. An M score of 12.8 was calculated using all test hours with $U > 6\,\mathrm{m\,s}^{-1}$.

(3) The model using the Petersen integral plume rise equations predicted maximum concentrations that were usually between a factor of 4 higher and a factor of 2 lower. An M score of 5 indicates that this model performed relatively better than the other two for this data set. If σ_z were underestimated by the modified Huber–Snyder equations used in these models then the plume rise predicted by this model is not necessarily more accurate.

(4) The models tended to perform better with higher wind speeds which resulted in higher concentrations.

(5) A wind tunnel investigation of dispersion with other wind directions at this site indicates that the dispersion process varies greatly depending on the orientation of the numerous buildings clustered around the source. The lower plume rise predicted by the Schulman–Scire downwashed plume rise equations results in much better model performance for north and west winds.

Our observations of dispersion near an Arctic industrial site emphasize the complex nature of building-influenced dispersion which has been recognized by previous investigators. Both plume rise and vertical diffusion at this site are greatly influenced by building-generated disturbances which are not adequately accounted for by the algorithms evaluated in this paper. It is also obvious that the Gaussian plume model framework is inadequate for simulating dispersion at this site and will not necessarily accurately predict maximum concentration even when reasonable estimates of plume rise and vertical diffusion can be provided. In view of these modeling limitations, we recommend that site-specific experimental data from wind tunnel or field studies may be used to verify predictions when buoyant plumes are released from low stacks near a clustered building complex. A potential alternative is the continued development of higher order, turbulence closure, numerical model techniques. Guenther et al. (1989) and Dawson (1987) have demonstrated success in numerically simulating the air flow reversal, mean streamline bending and increased turbulence levels which occur in a building wake and provide the information needed to estimate concentration distributions using finite difference techniques.

In the course of this field study, we noted that the highest hourly ground level tracer concentrations were associated with the high wind speeds of severe winter storms when human presence outside the gathering center is extremely limited. In addition, the tundra vegetation is inactive and covered with snow throughout the winter months. For these reasons, we feel that future investigations of air quality near Arctic industrial facilities should be directed towards identifying possible impacts during the short Arctic growing season. This requires quantification of wintertime pollutant deposition to the tundra snowfields, and determining the impact of any release when the snow melts, as well as direct deposition during summer. These efforts should be coordinated with investigations of the impact of specific air pollutants on the tundra ecosystem. A second area of potential concern which has not been adequately addressed by this or other field investigations is the possibility of adverse impacts on regional arctic air quality due to the long range transport of emissions from the oil gathering facilities.

REFERENCES

Benner R. and Lamb B. (1985) A fast response continuous analyzer for halogenated atmospheric tracers. *J. Atmos. Ocean. Technol* **2**, 582–589.

Berkowicz R. and Prahm L. (1982) Evaluation of the profile method for estimation of surface fluxes of momentum and heat. *Atmospheric Environment* **16**, 2809–2819.

Bowers J. F., Bjorkland J. R. and Cheney C. S. (1979) Industrial Source Complex (ISC) Dispersion Model User's Guide. Volume I, EPA-450/4-79-030, U.S. Environmental Protection Agency, Research Triangle Park, NC.

Briggs G. A. (1984) Plume rise and buoyancy effects. Atmospheric Science and Power Production, Randerson, D., Ed. DOE/TIC-27601, Technical Information Center, Oak Ridge, TN.

Dawson P. (1987) A numerical model to simulate the atmospheric transport and diffusion of pollutants over complex terrain. PhD Thesis, Washington State University, Pullman, WA.

Draxler R. R. (1976) Determination of atmospheric diffusion parameters. *Atmospheric Environment* **10**, 99–105.

Efron B. (1982) The jackknife, the bootstrap and other resampling plans. CBMS-NSF-38, Soc. for Ind. and Appl. Math., Philadelphia, PA.

Engineering Science (1980) Field validation of atmospheric dispersion models for natural gas compressor stations. AGA Catalog No. L51387. Prepared for the American Gas Association--Pipeline Research Committee, Arlington, VA.

Environmental Protection Agency (1981) Interim procedures for evaluating air quality models. Office of Air Quality Planning and Standards, Research Triangle Park, NC.

Fackrell J. E. (1984a) Parameters characterising dispersion in the near wake of buildings. *J. Wind Eng. Indust. Aero.* **16**, 97–118.

Fackrell J. E. (1984b) An examination of simple models for building influenced dispersion. *Atmospheric Environment* **18**, 89–98.

Guenther A., Allwine E., Bamesberger L., Friedman B. and Lamb B. (1988) Dispersion modeling in the Arctic, Quality Assurance Final Report (CR812775) to ASRL-EPA. Research Triangle Park, NC.

Guenther A. and Lamb B. (1989) Arctic dispersion modeling. Final report, EPA CR 812275-01, U.S. Environmental Protection Agency, Research Triangle Park, NC 27711.

Guenther A. and Lamb B. (1990) Atmospheric dispersion in the Arctic: winter-time boundary-layer measurements. *Boundary-Layer Met.* **49**, 339–366.

Guenther A., Lamb B. and Petersen R. (1989) Plume downwash and enhanced diffusion near buildings: comparison to wind tunnel observations for an Arctic industiral site. *J. appl. Met.* **28**, 343–353.

Guenther A., Lamb B. and Stock D. (1990) Numerical simulation of plume downwash at an Arctic industrial site. *J. appl. Met.* (in press).

Hanna S. R. and Heinold D. (1985) Development of a simple method for evaluating air quality models. API No. 4409, American Petroleum Institute, Washington D.C.

Hanzlick D., Schrader G. and Hachmeister L. (1988) Ice breakup/freezeup. 1987 Endicott Environmental Monitoring Program, Envirosphere Co., Anchorage, AK.

Haugen D. A. (1959) Project Prairie Grass, a Field Program in Diffusion. Geophysical Research Papers, No. 59, Vol. III. Report AFC RC-TR-58-235 (ASTIA Document AD-217076) Air Force Cambridge Research Center, MA.

Hosker R. P., Jr. (1984) Flow and diffusion near obstacles. In *Atmospheric Science and Power Production* (edited by Randerson D.). DOE/TIC-27601, Technical Information Center, Oak Ridge, TN.

Huber A. H. (1988a) Video images of smoke dispersion in the near wake of a model building. Part I. Temporal and spatial scales of vortex shedding. *J. Wind Engr. Ind. Aerodyn.* **31**, 189–223.

Huber A. H. (1988b) Evaluation of a method for estimating pollution concentrations downwind of influencing buildings. *Atmospheric Environment* **18**, 2313–2338.

Huber A. (1990) The influence of building width and orientation on plume dispersion in the wake of a building. *Atmospheric Environment* (in press).

Huber A. H. and Snyder W. H. (1982) Wind tunnel investigation of the effects of a rectangular-shaped building on dispersion of effluents from short adjacent stacks. *Atmospheric Environment* **17**, 2837–3848.

Krasnec J. D., Demaray D., Lamb B. and Benner R. (1984) Automated sequential syringe sampler for atmospheric tracer studies. *J. Atmos. Ocean Tech.* **1**, 372–378.

Petersen R. and Ratcliff M. (1988) Industrial source complex model with integral plume rise and dispersion enhacement (ISCIPRA) User's Guide, second edition, Volume I. CPP project 87-S-0187. American Petroleum Institute, Washington DC.

Radian Corporation and NHC Wind Engineering, Inc. (1985) The North Slope Air Quality Compliance Verification Project. Radian DCN 85-242-039-10-01, Houston, TX.

Richardson L. F. (1920) Some measurements of atmospheric turbulence. *Philos. Trans. R. Soc. London, Ser.* A **221**, 1–28.

Rickel C., Lamb B., Guenther A. and Allwine E. (1990) An infrared method for plume rise visualization and measurement. *Atmospheric Environment* (submitted).

Robins A. G. and Castro I. P. (1977) A wind tunnel investigation of plume dispersion in the vicinity of a surface mounted cube—II. The concentration field. *Atmospheric Environment* **11**, 299–311.

Schulman L. L. and Hanna S. R. (1986) Evaluation of Downwash modifications to the industrial source complex model. *J. Air Pollut. Control Ass.* **36**, 258–264.

Scire J. S. and Schulman L. L. (1980) Modeling plume rise from low-level buoyant line and point sources. *Proceedings of the Second Joint Conference on Applications of Air Pollution Meteorology*, New Orleans, LA.

Wagner C. P. (1987) Industrial Source Complex (ISC) Dispersion Model User's Guide Second Edition (Revised). Volume I, EPA-450/4-88-002, US Environmental Protection Agency, Research Triangle Park, NC.

Wilson D. and Chui (1987) Effect of turbulence from upwind buildings on exhaust gas dilution. *ASHRAEF Trans.* **93**, (Pt. 2).